6-24-2019

Nonlinear excitations in magnetic lattices with long-range interactions

Miguel Molerón
ETH Zürich

C. Chong
Bowdoin College

Alejandro J. Martínez
University of Oxford

Mason A. Porter
University of California, Los Angeles

P. G. Kevrekidis
University of Massachusetts Amherst

See next page for additional authors

New Journal of Physics
The open access journal at the forefront of physics
Deutsche Physikalische Gesellschaft DPG IOP Institute of Physics

PAPER • OPEN ACCESS

Nonlinear excitations in magnetic lattices with long-range interactions

To cite this article: Miguel Molerón *et al* 2019 *New J. Phys.* **21** 063032

IOP Publishing *New J Phys* **21** 2019) 063032 https: doi.org 10.1088 1367-2630 ab0118

New Journal of Physics

The open access journal at the forefront of physics

Deutsche Physikalische Gesellschaft DPG
IOP Institute of Physics

Published in partnership with: Deutsche Physikalische Gesellschaft and the Institute of Physics

CrossMark

OPEN CCESS

RECEIVED
7 December 2018

CCEPTED FOR PUBLIC TION
23 January 2019

PUBLISHED
24 June 2019

P PER

Nonlinear excitations in magnetic lattices with long range interactions

Miguel Molerón[1] **C Chong**[2,8] **Alejandro J Martínez**[3,7] **Mason A Porter**[4] **P G Kevrekidis**[5] and **Chiara Daraio**[6]

1 Institute of Geophysics, Department of Earth Sciences, ETH Zurich, 8092 Zurich, Switzerland
2 Department of Mathematics, Bowdoin College, Brunswick, ME 04011, United States of America
3 Oxford Centre for Industrial and Applied Mathematics, Mathematical Institute, University of Oxford, Oxford OX2 6GG, United Kingdom
4 Department of Mathematics, University of California, Los Angeles, CA 90095, United States of America
5 Department of Mathematics and Statistics, University of Massachusetts, Amherst, MA 01003, United States of America
6 Division of Engineering and Applied Science California Institute of Technology Pasadena, CA 91125, United States of America
7 Computational Biology Laboratory, Fundación Ciencia & Vida, 8320000, Santiago, Chile
8 Author to whom any correspondence should be addressed.

E mail: cchong@bowdoin.edu

Keywords: nonlinear lattice, breather, Fermi–Pasta–Ulam–Tsingou lattice, long-range interactions, non-local, defect, magnetic

Abstract

We study—experimentally, theoretically, and numerically—nonlinear excitations in lattices of magnets with long-range interactions. We examine breather solutions, which are spatially localized and periodic in time, in a chain with algebraically-decaying interactions. It was established two decades ago Flach 1998 *Phys Rev* E **58** R4116) that lattices with long-range interactions can have breather solutions in which the spatial decay of the tails has a crossover from exponential to algebraic decay. In this article, we revisit this problem in the setting of a chain of repelling magnets with a mass defect and verify, both numerically and experimentally, the existence of breathers with such a crossover.

Introduction

There has been considerable progress in understanding localization in nonlinear lattices over the past three decades 1]. A prototypical example are spatially localized and temporally periodic discrete breathers or just 'breathers) 2]. The span of systems in which breathers have been studied is broad and diverse. They include optical waveguide arrays and photorefractive crystals 3], micromechanical cantilever arrays 4], Josephson-junction ladders 5, 6], layered antiferromagnetic crystals 7, 8], halide-bridged transition-metal complexes 9], dynamical models of the DNA double strand 10], Bose–Einstein condensates BECs) in optical lattices 11], and many others. Many of these studies concern models with coupling between elements only in the form of nearest-neighbor interactions. However, there has been a great deal of theoretical and computational work in lattices with interactions beyond nearest neighbors. For example, some models of polymers 12], quantum systems 13]; and optical waveguide arrays 14, 15] have included interactions beyond nearest neighbors; see also 16, 17]. Dynamical lattices with long-range interactions e.g. with all-to-all coupling) have been used as models for energy and charge transport in biological molecules 18]; and studies of such long-range models have explored phenomena such as equilibrium relaxation 19], thermostatistics 20], chaos 21, 22], and energy thresholds 23, 24]. Oscillators of numerous varieties have also been coupled via long-range interactions on lattices and more general network structures) 25, 26]. In fact, until recently, they were often assumed to be a fundamental ingredient for the formation of so-called 'chimera states 27–29].

Long-range interactions can have a signi cant effect on nonlinear excitations and yield phenomena that are rather different from those that result from only nearest-neighbor coupling. For example, stationary solitary waves with a nontrivial phase can arise both in discrete nonlinear Schrödinger DNLS) equations with next-nearest-neighbor NNN) interactions 16, 30] and in NNN discrete Klein–Gordon KG) 31] equations, and bistability of solitary waves is possible in DNLS equations with long-range interactions [32, 33]. Finally, and most relevant for the present paper, breathers in KG and Fermi–Pasta–Ulam–Tsingou (FPUT) lattices with long-range interactions can exhibit a crossover from exponential decay (at short distances from the breather center) to algebraic decay (at long distances) if the interactions decay significantly slowly (specifically, algebraically slowly) [24]. A variety of new studies continue to elucidate fascinating consequences of long-range interactions. For example, recent studies have revealed the emergence of traveling discrete breathers without tails in nonlinear lattices with suitable long-range interactions [34] and the emergence of a linear spectral gap, which enables the emergence of a low-frequency breather [35], in nonlinear lattices with other long-range interactions. Although there are many theoretical and computational studies of lattice systems with long-range interactions, we are not aware of any experimental realizations of breathers in such systems.

In this paper, we use experiments, theory, and numerical computations to study a strongly nonlinear lattice with long-range interactions that decay algebraically. Specifically, we consider a one-dimensional chain of repelling magnets with a single mass defect. This system allows us to realize fundamental structures, such as solitary waves, in a tabletop setup with real-time spatio-temporal resolution [36, 37]. Moreover, the use of magnetic interactions allows exciting applications. They have already been used as a passive mechanism to couple nodes of a lattice for unidirectional wave-guiding [38]; and it has been suggested that magnetic interactions can be used to design novel devices for frequency conversion [39] and shock absorption [36]. In our study, we focus on breathers in a magnetic chain and demonstrate that there is a crossover from exponential decay to algebraic decay in the spatial profile of these breathers.

Experimental setup

In figure 1(a), we show a picture of our experimental setup. We situate an array of disc magnets over a 150 mm × 300 mm rectangular air-bearing table from IBS Precision Engineering (to reduce surface friction) and between two Teflon rectangular rods (to restrict the particle motion to one dimension). As shown in the inset of figure 1(a), we insert each magnet into a 3D-printed support. We glue a glass slide below the 3D-printed support to obtain a desired amount of levitation. The magnets are axially magnetized, and they have the same orientation, so each magnet repels its neighbors. The mean mass of the non-defect particles in the 25-particle chain is $M = 0.45$ g (with a standard deviation of $s = 0.0028$), and the mass of the defect particle is $m = 0.20$ g. The distance between the boundary particles is $L \approx 33.7$ cm. To excite the chain harmonically, we glue the left boundary to an aluminum bar attached to an electrodynamic transducer (Beyma 5MP60/N). The measured total harmonic distortion of this transducer is below 10% in the amplitude range (between 0 and 4 cm) under consideration.

We measure the motion using digital-image-correlation (DIC) software from Correlated Solutions (VIC 2D). We use a camera (of model GS3-U3-41C6C-C from Point Gray) to record the particles' motion at a frame rate of 200 fps. To help track the particles, we glue speckle patterns to the top of the 3D-printed support (see figure 1(a)). We postprocess the video files with the VIC software to extract particle displacements and velocities. As in [36, 38], we assume that the relationship between the repelling force and distance has the form $F = Ad^p$, where F is the force and d is the center-to-center separation distance between two particles. We estimate the magnetic coefficient A and exponent p by measuring the repelling force at 22 separation distances (represented by plus signs in figure 1(b)). We measure the repelling force by fixing one magnet to a load cell (of type OMEGA LCL-113G) and approaching another magnet using a high-precision translation stage. Using a least-squares fitting routine for $\log(F)$ versus $\log(d)$ with our experimental data (see the inset in figure 1(b)) yields $A \approx 1.5683 \times 10^{-12} N\ m^{-p}$ and $p \approx -4.473$. We use these parameter values throughout the text.

Theoretical setup

Our experimental setup motivates the following model (which assumes that each node, representing a magnet, is coupled to every other node in a chain):

$$M_n \ddot{u}_n = \sum_{j=1}^{\infty} [A(j\delta_0 + u_n - u_{n-j})^p - A(j\delta_0 + u_{n+j} - u_n)^p] - \eta \dot{u}_n , \qquad (1)$$

where $u_n = u_n(t) \in \mathbb{R}$ is the displacement of the nth magnet from its equilibrium position, the mass of the nth magnet is M_n, the magnetic coefficient is A, and the nonlinearity exponent is p. In figure 1(b), we show the spatial decay in the force with respect to the center-to-center distance between particles. This model assumes that each magnet, including its magnetic properties, is identical. The equilibrium separation distance between two adjacent magnets in an infinite lattice is δ_0. In a finite lattice, the equilibrium separation distance depends on the

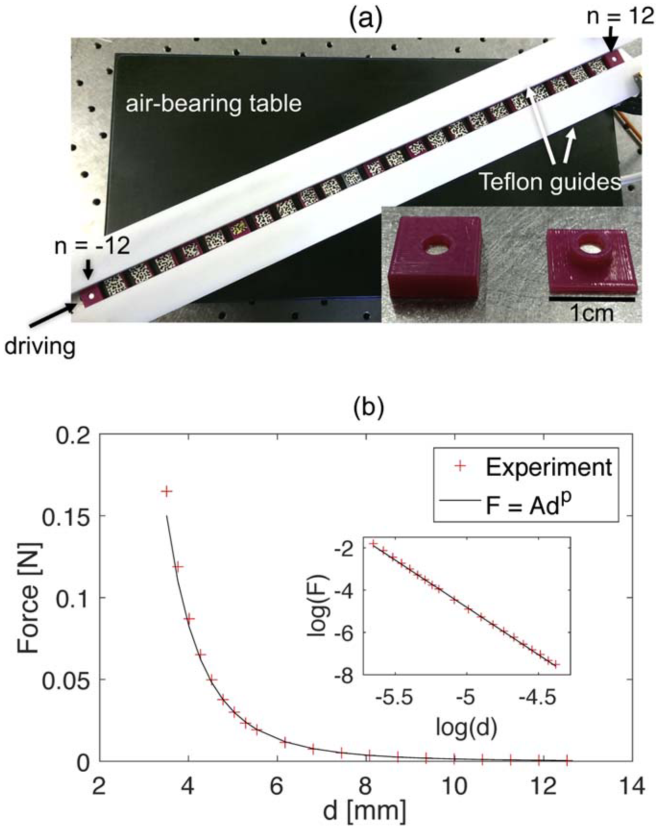

Figure 1. a) Picture of our experimental setup. The lattice consists of 25 magnetic particles deposited on an air-bearing table. The right boundary $n = 12$) is xed, and the left boundary $n =$ 12) is driven harmonically with an electrodynamic transducer. The magnetic particles are composed of a disc magnet type Supermagnete S-03-01-N, with magnetization grade N48, a diameter of 3 mm, and a height of 1 mm). The inset shows a magni ed view of the magnetic particles embedded in a 3D-printed support: left) normal particle and right) defect particle. b) Relationship between the force F and center-to-center separation distance d between two particles. The plus signs represent experimental data, and the solid curve represents a functional form $F = Ad^p$. In the inset, we show a plot of $\log(F)$ versus $\log(d)$ that we use for tting the exponent p and the magnetic coef cient A.

lattice location; see Appendix A for details. We model damping effects with a dashpot term $\eta\dot{u}_n$, where we empirically estimate the damping factor see our discussion below). We apply a harmonic boundary drive $u_{\mathrm{left}}(t) = a\sin(2\pi f_b t)$, where a denotes the drive amplitude and f_b denotes its frequency. Our initial theoretical considerations involve a Hamiltonian lattice, so we take $a =$ $= 0$. Later, when we compare our numerical results to experiments, we also consider nonzero values of the drive amplitude and damping factor.

In a homogeneous chain where all masses are identical, so $M_n = M$) the linearization of 1) has plane-wave solutions $u_n = \exp(\mathrm{i}kn + \mathrm{i}\omega t)$, where

$$\omega^2(k) = K_2 \sum_{j=1}^{\infty} \frac{1}{j^s}[1 - \cos(jk)] = K_2[\zeta(s) - \mathrm{Re}\{\mathrm{e}^{\mathrm{i}k}\phi(\mathrm{e}^{\mathrm{i}k}, s, 1)\}], \quad (2)$$

where $s = 1$ p, the linear stiffness is $K_2 = -2Ap\delta_0^{p-1}/M$, the Riemann zeta function is $\zeta(s)$, and $\phi(z, s, a)$ is the Hurwitz–Lerch transcendent function 40]. This dispersion curve is nonanalytic in the wavenumber k, because its κth derivative where κ is the integer satisfying $s - 1 \leqslant \kappa < s$) with respect to k is discontinuous at $k = 0$. Below we discuss the consequences of this nonanalyticity. The dispersion curve is analytic at the upper band edge i.e. at $k = \pi$).

Because we are interested in solutions that decay spatially to 0 at in nity, it is natural to seek breather frequencies that lie above the spectrum edge $\omega(\pi)$ to avoid resonances with linear modes). Equation 1) with $M_n = M$ is not an appropriate model for seeking small-amplitude bright) breather solutions, because one needs the plane waves to have a modulational instability, which is not possible in a homogeneous magnetic chain 2]. Hence, to obtain breathers, we break the uniformity of the chain by introducing a light-mass defect, motivated by the analysis of 41] for nonlinear lattices with nearest-neighbor interactions. This creates a defect mode that lies above the edge of the linear spectrum, from which breathers can bifurcate. Breathers in nearest-neighbor FPUT-like lattices with defects have been studied extensively both theoretically 41] and experimentally 42]. To nd breathers in a magnetic chain, one can alternatively use a lattice with spatial heterogeneity e.g. a dimer) 43–45] or one with an on-site potential 46, 47] or local resonators 48, 49].

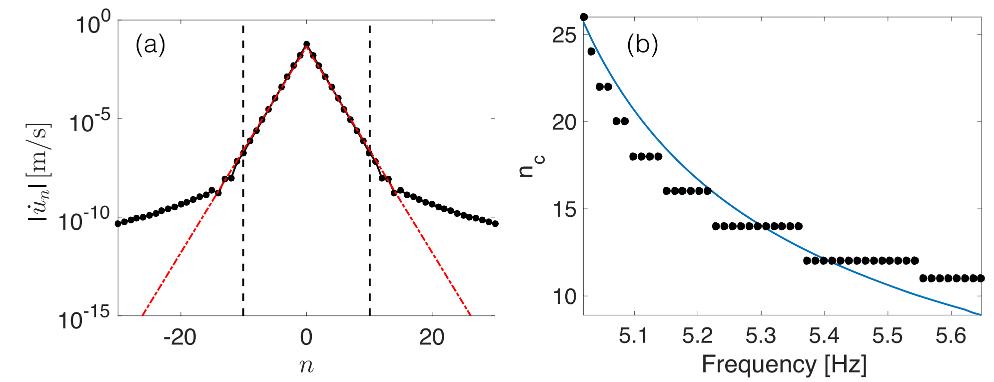

Figure 2. a) Semi-log plot of a breather solution black curve with markers), with a frequency of $f_b \approx 5.54$ Hz, of equation 1) with $= a = 0$ for a magnetic chain with a defect particle in the center $n_d = 0$). The vertical axis gives the absolute value of the velocity, and the horizontal axis gives the node index. For comparison, we show a breather solution of the same frequency for a lattice with only nearest-neighbor interactions dashed–dotted red curve). The vertical dashed line is the predicted value of the crossover value n_c from equation 4). b) Numerically computed crossover point black markers) and prediction based on equation 4) curve).

A chain with a single mass defect is the starting point for our model with long-range interactions. We reduce the mass of the n_dth node but without modifying its magnetic properties) by adjusting the support in which the magnet is embedded see gure 1 b)). Consequently, $M_{n_d} = m$, where m is the mass of the defect; and $M_n = M$ for $n \neq n_d$, where M is the mass of the non-defect particles.

Numerical results

We start by numerically computing time-periodic solutions of the Hamiltonian variant of equation 1) i.e. with $a = \quad = 0$) and $N = 65$ particles. The values that we use for the magnetic potential parameters are $A \approx 1.5683 \times 10^{-12} N/m^p$ and $p \approx \quad 4.473$. Each particle, except for the defect in the center, has a mass of $M = 0.45$ g; the mass of the defect particle is $m = 0.20$ g. The numerical value of the equilibrium distance that we use is $\delta_0 \approx 1.4042$ cm. We numerically compute the linear spectrum and obtain a defect mode with frequency $f_d \approx 5.66$ Hz. We use this linear mode as an initial guess in a Newton method and identify a time-periodic solution with a frequency slightly below the defect frequency. See Appendix B for details on numerical computations. In gure 2 a), we show a semi-log plot of the absolute value of the velocity pro le of the breather that we obtain using Newton iterations. One of the de ning features of a breather in lattices with nearest-neighbor interactions is exponential decay of the tails. See the dashed red curve in gure 2 a).) The linear slope of the breather in the semi-log plot suggests that there is exponential decay of the tail close to the center. In fundamental contrast to its nearest-neighbor counterpart, the breather in the lattice with long-range interactions exhibits a transition at a critical lattice site n_c, and the decay becomes algebraic rather than exponential. This feature was rst observed about two decades ago in a KG lattice with a cubic potential i.e. in the ϕ^4 model) 24], which has long-range interactions with coef cients with algebraic decay. In particular, they have a power-law decay $\mathcal{O}(1/n^s)$ with respect to particle n. The linearization of equation 1) also has interaction coef cients with power-law decay $\mathcal{O}(1/n^s)$. The algebraic decay of the breather far away from its center arises as follows; see 24] for details. Its amplitude is small away from its center, so we can linearize the equations of motion. Additionally, because the breather is temporally periodic, we can express the time dependence of the solution as a Fourier series: $u_n(t) = \sum_j \hat{u}_n(j) e^{ij\omega_b t}$, where $\omega_b = 2\pi f_b$ is the breather s angular frequency. One computes the Fourier coef cients using Green s functions 24] to obtain

$$\hat{u}_n(j) = \int_0^{2\pi} \frac{\cos(kj)}{(j\omega_b)^2 - \omega^2(k)} \, dk, \tag{3}$$

where $\omega^2(k)$ is given by the dispersion relation in equation 2). Now it is clear why it is important to highlight the nonanalytic nature of $\omega^2(k)$: the Fourier coef cients in equation 3) with discontinuities in the κth derivative yield Fourier series that converge algebraically. This implies that $u_n \sim 1/n^s$ for large n 24]. One can make similar arguments to explain the exponential decay near the center; see 24] for details.

Assuming that the proportionality constants of the exponential decay and the algebraic decay are roughly the same, there is a crossover point between the two types of decay that satis es $e^{-\nu n_c} = \frac{1}{n_c^s}$, where ν is the exponential decay rate of the breather near the center. This yields the following prediction for the crossover site n_c 24]:

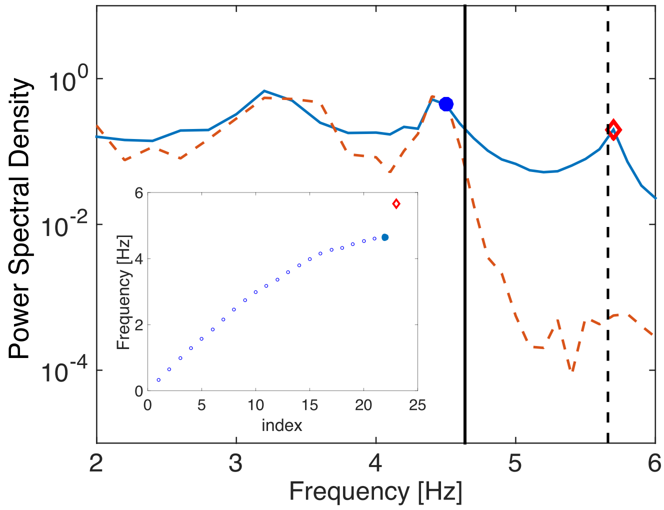

Figure 3. Experimental power spectral density PSD) for a homogeneous chain of 25 magnets dashed red curve) and for a magnetic chain with a mass defect located at site $n_d =$ 8 solid blue curve). The experimental cutoff frequency blue disc) and defect mode red diamond) are in reasonable agreement with the numerical prediction vertical solid and dashed lines). In the inset, we show numerically computed eigenfrequencies versus the eigenfrequency index for a chain with 23 particles 25 including the two xed boundaries) and a single defect at site $n_d = -8$ and no damping or driving $= a = 0$). In the inset, we order the modes based on the values of their frequencies. The blue disc in the inset represents the numerical cutoff frequency, and the red diamond shows the numerical defect mode.

$$\frac{\log n_c}{n_c} = \frac{\nu}{1 - p}. \tag{4}$$

For the solution in gure 2 a), the predicted crossover is $n_c = 10$, which is roughly where the decay properties change in the numerical solution see gure 2 a)). To validate equation 4), we compute the crossover point from the numerically-obtained breather solutions. We calculate this point numerically by determining the rst particle at which the deviation of the solution from the best- t line in the semi-log scale exceeds 1 of the solution amplitude. In the example in gure 2 a), this yields a crossover point of $n_c = 12$. Equation 4) predicts that the crossover location depends on the solution s exponential decay rate ν, which in turn depends on the breather frequency f_b. In gure 2 b), we show a comparison of observed numerical crossovers and equation 4) for various breather frequencies.

Experimental results

For our experiments, we consider a chain of $N = 25$ magnets including the boundaries) with a defect magnet at site $n_d =$ 8. We experimentally probe the linear spectrum by performing a frequency sweep. To do this, we excite the chain at 33 frequencies between 2 and 6 Hz and extract the resulting steady-state displacement amplitudes at the excitation frequency in different locations. The dashed red curve in gure 3 represents the power spectral density PSD) of particles 4 to 0, and the solid blue curve represents the PSD of the defect particle. The model prediction based on the Hamiltonian limit i.e. with $= a = 0$) of equation 1) which we computed numerically, as shown in the inset of gure 3) agrees with the experimentally-observed passband cutoff frequency $f \approx 4.50$ Hz and defect-mode frequency $f_d \approx 5.66$ Hz.

To further evaluate our model, we initialize the experimental chain using the displacements that correspond to the theoretically-predicted Hamiltonian breather with frequency $f_b \approx 5.46$ Hz. The nodes oscillate initially with the predicted frequency see gure 4 a)). In this particular experiment, we do not add energy to the system. Thus, as the oscillation amplitude decreases due to damping, the dynamics gradually becomes more linear and the oscillation frequency approaches the sole linear defect-mode frequency $f_d \approx 5.66$ Hz. We use this experiment to empirically determine the damping parameter ≈ 0.10 g s 1 to match the temporal amplitude decay of the defect particle. See the inset in gure 4 a).) We conduct an analogous numerical experiment using equation 1) with damping but no driving speci cally, $= 0.10$ g s 1 and $a = 0$), which matches the observed experimental data; see the solid red discs in gure 4 a).

Our nal experiment probes the decay properties of the breather. To allow the experimental system to reach a steady state which allows us to more closely examine the decay properties), we again continuously harmonically excite the left boundary magnet, so the displacement of the boundary magnet is $u_{\text{left}} = a \sin(2\pi f_b)$. We thereby treat the boundary as a 'core of the breather, so we do not use a defect particle in these experiments. We seek

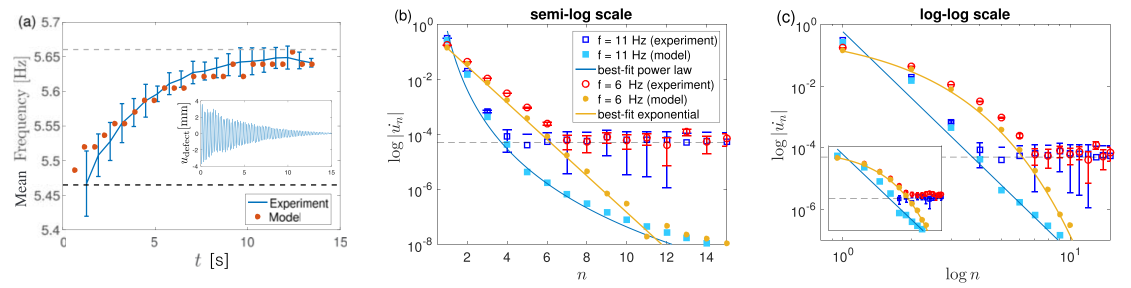

Figure 4. a) Experiment initialized with a Hamiltonian breather solution of equation 1) with frequency $f_b \approx 5.46$ Hz. We show the mean oscillation frequency of the defect particle for every 1.28 s for the experiment blue markers with error bars) and model with damping with $= 0.10$ g s ^{1}) but no driving red discs). The error bars indicate the standard deviation over 5 experimental realizations. Note that the defect particle oscillates initially at the predicted frequency. The frequency approaches the sole defect frequency of the linear system, as the damping causes displacements to approach 0. In the inset, we show an example of defect-particle decay from an experiment. b) Semi-log plot of the experimental data for drive frequencies of $f_b = 6$ Hz open red circles with error bars) and $f_b = 11$ Hz open blue squares with error bars). The chain is homogeneous there is no defect particle), because the boundary drive is acting like a defect particle which we label as $n = 0$). We show our predictions from the damped, driven model lled markers) as well as the best t to exponential yellow curve) and power-law blue curve) decay. The experimental data for $f_b = 6$ Hz follows a roughly linear trend in the semi-log plot, suggesting that its decay is exponential. c) Same as panel b) but as a log–log plot. The experimental data for $f_b = 11$ Hz follows a roughly linear trend in the log–log plot, suggesting that its decay is algebraic. Panels b) and c) share the legend that we show in b). The inset in panel c) shows a similar result for a chain of length $N = 29$ which has a smaller equilibrium distance). In this case, more particles have an amplitude that is comparable to the amount of noise.

time-periodic solutions of equation 1) that account for both the boundary excitation and damping effects. We use the parameter values $= 0.10$ g s ^{1} and $a = 3.8$ mm. The transition that we observe in gure 2 a) occurs at amplitudes, which we estimate to be 0.05 mm s ^{1}, that lie below the amount of noise in the experiments. This value corresponds to the mean velocity amplitudes of particles 9–24, whose motion can be attributed primarily to ambient vibrations. Thus, for the drive breather) frequency $f_b = 6$ Hz, we observe only exponential decay.

However, for a drive frequency of $f_b = 11$ Hz, the transition to algebraic decay occurs close to the core of the breather, so there appears to be a glimpse of the associated decay prior to reaching the level at which ambient noise vibrations overwhelm the algebraic tail. Note that the crossover approaches the core of the breather as the breather frequency increases see gure 2 b)). In gures 4 b), c), we show the tails of the breather in semi-log and log–log plots. For $f_b = 6$ Hz, the experimental data open red circles with error bars) has a roughly linear trend in the semi-log plot, suggesting that its decay is exponential. The experimental data follows the model prediction solid yellow circles) up to the point at which it reaches the noise level the horizontal dashed gray line). We t using a least-squares procedure) the model solution with an exponential curve of the form $\alpha e^{-\beta n}$ solid yellow curve), and we obtain $\alpha \approx 0.6287$ and $\beta \approx 1.529$. For $f_b = 11$ Hz, the experimental data open blue squares with error bars) has a roughly linear trend in a log–log plot, suggesting its algebraic decay. The experimental data follows our model s prediction solid light blue squares) until reaching the noise level horizontal dashed gray line). We t the model solution with a power-law curve of the form $\alpha n^{-\beta}$ solid blue curve), and we obtain $\alpha \approx 0.579$ and $\beta \approx 7.131$. Our results for other parameter values are similar. For example, in the inset of gure 4 c), we show a log–log plot of periodic solutions with $f_b = 9$ Hz red) and $f_b = 13$ Hz blue) for a chain with $N = 29$ particles. Because the lattice is con ned to a length of $L \approx 33.7$ cm, the equilibrium distance is about 6 7 of the one in the $N = 25$ chain. This increases the linear stiffness and hence increases the passband cutoff. Consequently, we need higher frequencies to avoid resonance with the linear modes.

Discussion and conclusions

We studied a lattice of magnets with long-range interactions, and we obtained quantitative agreement between theory, numerics, and experiment. Speci cally, using a combination of experiments, computation, and analysis, we explored the prediction of 24], made about twenty years ago, that the tail of a breather solution of this nonlinear lattice exhibits a transition from exponential to algebraic decay. As far as we are aware, our work represents the rst experimental realization of breathers in a nonlinear lattice with long-range interactions.

The study of long-range interaction systems is an increasingly important topic in numerous and wide-ranging areas of physics. These include dipolar BECs 50], where the recent formation of quantum droplets and their bound states 51] suggests that interesting types of long-range interactions can also arise in the study of BECs in optical lattices. Long-range interactions also play important roles in the study of coupled phase oscillators in diverse physical settings 26], heat transport in oscillator chains coupled to thermal reservoirs 52, 53], and more.

Our experimental system provides a new platform for the manifestation of breathers. It differs in a fundamental way from standard setups, in which only nearest-neighbor interaction are possible, and it allows one to experimentally observe novel dynamical behavior. In addition to our observations in the present paper, our work paves the way towards further studies to explore the nuances of long-range interactions in nonlinear lattice systems. Examples include bistability of solitary waves 32, 33], solitary waves with nontrivial phases 31], and low-frequency breathers 35]. These avenues go beyond the con nes of mechanical or magnetic systems and are of broad appeal for a variety of long-range phenomena. It would be especially interesting to examine what happens when breathers interact and how the decay properties and interactions between breathers) depend on lattice dimensionality.

Acknowledgments

This material is based upon work supported by the National Science Foundation under Grant No. DMS-1615037 CC), DMS-1809074 PGK), and EFRI Grant No. 1741565 CD). AJM acknowledges support from CONICYT BCH72130485 2013), Proyecto de FinanciamientoBasal PFB16, and Apoyo a Centros Tecnológicos con Financiamiento Basal AFB 170004. PGK gratefully acknowledges support from the US-AFOSR via FA9550-17-1-0114. MAP thanks C. J. Lustri for insightful discussions.

Appendix A. Equations of motion in a nite chain

In a chain of N where N is odd) magnets that we arrange as a lattice con ned within a distance $L \in \mathbb{R}$ with xed boundary conditions i.e. $u_n = 0$ for particles $n = -\frac{N+1}{2}, \frac{N+1}{2}$) the equilibrium distance between magnets $n-1$ and n depends on n. The $N+1$ equilibrium distances $\delta_{0,n}$ with $n \in \{-\frac{N-1}{2}, \ldots, \frac{N+1}{2}\}$) satisfy

$$L = \sum_{n=-\frac{N-1}{2}}^{\frac{N+1}{2}} \delta_{0,n}$$

and the following N equations:

$$0 = \sum_{j=-\frac{N+1}{2}}^{n-1} \left(\sum_{i=j+1}^{n} \delta_{0,i} \right)^p - \sum_{j=n+1}^{\frac{N+1}{2}} \left(\sum_{i=n+1}^{j} \delta_{0,i} \right)^p, \tag{5}$$

where $n \in \{-\frac{N-1}{2}, \ldots, \frac{N-1}{2}\}$. We model damping effects with a dashpot term $\eta \dot{u}_n$, where we empirically estimate the damping factor . We apply a harmonic boundary drive $u_{\mathrm{left}}(t) = a \sin(2\pi f_b t)$, where a denotes the drive amplitude and f_b denotes its frequency. Thus, for a nite chain, we obtain the following N equations of motion:

$$M_n \ddot{u}_n = \sum_{j=-\frac{N+1}{2}}^{n-1} A \left(\sum_{i=j+1}^{n} [\delta_{0,i}] + u_n - u_j \right)^p - \sum_{j=n+1}^{\frac{N+1}{2}} A \left(\sum_{i=n+1}^{j} [\delta_{0,i}] + u_j - u_n \right)^p - \eta \dot{u}_n, \tag{6}$$

with $n \in \{-\frac{N-1}{2}, \ldots, \frac{N-1}{2}\}$ and the boundary conditions

$$u_{-\frac{N+1}{2}}(t) = a \sin(2\pi f_b t), \quad u_{\frac{N+1}{2}}(t) = 0.$$

For an in nite lattice i.e. in the limit $N \to \infty$) the equilibrium distances are constant with respect to lattice site. This is easily veri ed by substituting $\delta_{0,n} = \delta_0$ into equation 5):

$$\begin{aligned} \sum_{j=-\infty}^{n-1} ((n-j)\delta_0)^p - \sum_{j=n+1}^{\infty} ((j-n)\delta_0)^p &= \sum_{j=1-n}^{\infty} ((j+n))^p - \sum_{j=n+1}^{\infty} ((j-n))^p \\ &= \sum_{k=1}^{\infty} (k)^p - \sum_{\ell=1}^{\infty} (\ell)^p = 0, \end{aligned}$$

where we de ned new indices $k = j \quad n$ and $\quad = j \quad n$. Substituting $\delta_{0,n} = \delta_0$ into equation 6) and rede ning indices once again leads to equation 1), which is valid for an in nite lattice.

Appendix B. Numerical methods

We find time-periodic solutions of equation (6) with period T by numerically computing roots x^0 of the map $f(x^0) = x^0 - \tilde{x}^0(T)$, where x^0 is the initial value of equation (6) and $\tilde{x}^0(T)$ is the solution at time T of equation (6) with initial value x^0. See [2] for details. We numerically integrate equation (6) with an adaptive-size Runge–Kutta method. We use the linearization of (6) to determine our initial guess for the Newton iterations.

ORCID iDs

P G Kevrekidis https://orcid.org/0000-0002-7714-3689

References

[1] Kevrekidis P G 2011 *IMA J. Appl. Math.* **76** 389
[2] Flach S and Gorbach A 2008 *Phys. Rep.* **467** 1
[3] Lederer F, Stegeman G I, Christodoulides D N, Assanto G, Segev M and Silberberg Y 2008 *Phys. Rep.* **463** 1
[4] Sato M, Hubbard B E and Sievers A J 2006 *Rev. Mod. Phys.* **78** 137
[5] Binder P, Abraimov D, Ustinov A V, Flach S and Zolotaryuk Y 2000 *Phys. Rev. Lett.* **84** 745
[6] Trías E, Mazo J J and Orlando T P 2000 *Phys. Rev. Lett.* **84** 741
[7] English L Q, Sato M and Sievers A J 2003 *Phys. Rev.* B **67** 024403
[8] Schwarz U T, English L Q and Sievers A J 1999 *Phys. Rev. Lett.* **83** 223
[9] Swanson B I, Brozik J A, Love S P, Strouse G F, Shreve A P, Bishop A R, Wang W-Z and Salkola M I 1999 *Phys. Rev. Lett.* **82** 3288
[10] Peyrard M 2004 *Nonlinearity* **17** R1
[11] Morsch O and Oberthaler M 2006 *Rev. Mod. Phys.* **78** 179
[12] Hennig D 2001 *Eur. Phys. J.* B **20** 419
[13] Choudhury A G and Chowdhury A Roy 1996 *Phys. Scr.* **53** 129
[14] Efremidis N K and Christodoulides D N 2002 *Phys. Rev.* E **65** 056607
[15] Kevrekidis P G, Malomed B A, Saxena A, Bishop A R and Frantzeskakis D J 2003 *Physica* D **183** 87
[16] Kevrekidis P G 2009 *Phys. Lett.* A **373** 3688
[17] Kevrekidis P G 2013 *J. Opt.* **15** 044013
[18] Mingaleev S F, Christiansen P L, Gaididei Y B, Johansson M and Rasmussen K Ø 1999 *J. Biol. Phys.* **25** 41
[19] Miloshevich G, Nguenang J-P, Dauxois T, Khomeriki R and Ruffo S 2015 *Phys. Rev.* E **91** 032927
[20] Christodoulidi H, Tsallis C and Bountis T 2014 *Europhys. Lett.* **108** 40006
[21] Zaslavsky G M, Edelman M and Tarasov V E 2007 *Chaos* **17** 043124
[22] Korabel N and Zaslavsky G M 2007 *Physica* A **378** 223
[23] Kastner M 2004 *Nonlinearity* **17** 1923
[24] Flach S 1998 *Phys. Rev.* E **58** R4116
[25] Porter M A and Gleeson J P 2016 *Dynamical Systems on Networks: A Tutorial (Frontiers in Applied Dynamical Systems: Reviews and Tutorials)* vol 4 (Cham: Springer)
[26] Arenas A, Díaz-Guilera A, Kurths J, Moreno Y and Zhou C 2008 *Phys. Rep.* **469** 93
[27] Xie J, Knobloch E and Kao H-C 2014 *Phys. Rev.* E **90** 022919
[28] Xie J, Knobloch E and Kao H-C 2015 *Phys. Rev.* E **92** 042921
[29] Panaggio M J and Abrams D M 2015 *Nonlinearity* **28** R67
[30] Chong C, Carretero-Gonázlez R, Malomed B A and Kevrekidis P G 2011 *Physica* D **240** 1205
[31] Koukouloyannis V, Kevrekidis P G, Cuevas J and Rothos V 2013 *Physica* D **242** 16
[32] Gaididei Y B, Mingaleev S F, Christiansen P L and Rasmussen K Ø 1997 *Phys. Rev.* E **55** 6141
[33] Rasmussen K Ø, Christiansen P, Johansson M, Gaididei Y and Mingaleev S 1998 *Physica* D **113** 134
[34] Doi Y and Yoshimura K 2016 *Phys. Rev. Lett.* **117** 014101
[35] Yamaguchi Y and Doi Y 2018 *Phys. Rev.* E **97** 062218
[36] Molerón M, Leonard A and Daraio C 2014 *J. Appl. Phys.* **115** 184901
[37] Mehrem A, Jiménez N, Salmerón-Contreras L J, García-Andrés X, García-Raffi L M, Picó R and Sánchez-Morcillo V J 2017 *Phys. Rev.* E **96** 012208
[38] Nadkarni N, Arrieta A F, Chong C, Kochmann D M and Daraio C 2016 *Phys. Rev. Lett.* **116** 244501
[39] Serra-Garcia M, Molerón M and Daraio C 2018 *Phil. Trans.* A **376** 20170137
[40] Erdélyi A, Magnus W, Oberhettinger F and Tricomi F 1981 *Higher Transcendental Functions* (Melbourne: Krieger)
[41] Theocharis G, Kavousanakis M, Kevrekidis P G, Daraio C, Porter M A and Kevrekidis I G 2009 *Phys. Rev.* E **80** 066601
[42] Boechler N, Theocharis G and Daraio C 2011 *Nat. Mater.* **10** 665
[43] Theocharis G, Boechler N, Kevrekidis P G, Job S, Porter M A and Daraio C 2010 *Phys. Rev.* E **82** 056604
[44] Boechler N, Theocharis G, Job S, Kevrekidis P G, Porter M A and Daraio C 2010 *Phys. Rev. Lett.* **104** 244302
[45] Huang G and Hu B 1998 *Phys. Rev.* B **57** 5746
[46] James G 2011 *Math. Models Methods Appl. Sci.* **21** 2335
[47] James G, Kevrekidis P G and Cuevas J 2013 *Physica* D **251** 39
[48] Liu L, James G, Kevrekidis P G and Vainchtein A 2016a *Nonlinearity* **29** 3496
[49] Liu L, James G, Kevrekidis P G and Vainchtein A 2016b *Physica* D **331** 27
[50] Lahaye T, Menotti C, Santos L, Lewenstein M and Pfau T 2009 *Rep. Prog. Phys.* **72** 126401
[51] Ferrier-Barbut I, Kadau H, Schmitt M, Wenzel M and Pfau T 2016 *Phys. Rev. Lett.* **116** 215301
[52] Olivares C and Anteneodo C 2016 *Phys. Rev.* E **94** 042117
[53] Iubini S, Cintio P D, Lepri S, Livi R and Casetti L 2018 *Phys. Rev.* E **97** 032102